JES Focus Issue on Lithium–Sulfur Batteries: Materials, Mechanisms, Modeling, and Applications

Irreversible vs Reversible Capacity Fade of Lithium-Sulfur Batteries during Cycling: The Effects of Precipitation and Shuttle

Monica Marinescu,[a,z] Laura O'Neill,[b] Teng Zhang,[a] Sylwia Walus,[b] Timothy E. Wilson,[c] and Gregory J. Offer[a]

[a]*Department of Mechanical Engineering, Imperial College London, SW7 2AZ, United Kingdom*
[b]*OXIS Energy Ltd, E1 Culham Science Centre, Abingdon, Oxfordshire, OX14 3DB, United Kingdom*
[c]*Physics Department, Forest School, London E17 3PY, United Kingdom*

Lithium-sulfur batteries could deliver significantly higher gravimetric energy density and lower cost than Li-ion batteries. Their mass adoption, however, depends on many factors, not least on attaining a predictive understanding of the mechanisms that determine their performance under realistic operational conditions, such as partial charge/discharge cycles. This work addresses a lack of such understanding by studying experimentally and theoretically the response to partial cycling. A lithium-sulfur model is used to analyze the mechanisms dictating the experimentally observed response to partial cycling. The zero-dimensional electrochemical model tracks the time evolution of sulfur species, accounting for two electrochemical reactions, one precipitation/dissolution reaction with nucleation, and shuttle, allowing direct access to the true cell state of charge. The experimentally observed voltage drift is predicted by the model as a result of the interplay between shuttle and the dissolution bottleneck. Other features are shown to be caused by capacity fade. We propose a model of irreversible sulfur loss associated with shuttle, such as caused by reactions on the anode. We find a reversible and an irreversible contribution to the observed capacity fade, and verify experimentally that the reversible component, caused by the dissolution bottleneck, can be recovered through slow charging. This model can be the basis for cycling parameters optimization, or for identifying degradation mechanisms relevant in applications. The model code is released as Supplementary material B.

 [DOI: 10.1149/2.0171801jes]

Manuscript submitted August 22, 2017; revised manuscript received November 7, 2017. Published December 30, 2017. *This paper is part of the JES Focus Issue on Lithium-Sulfur Batteries: Materials, Mechanisms, Modeling, and Applications.*

Lithium sulfur (LiS) batteries have the potential to provide a step change in performance, compared to Li-ion batteries, with an expected practical energy density of 700 Wh kg^{-1} compared to that of the intercalation Li-ion batteries, of 210 Wh kg^{-1}.[1,2] Added benefits, such as a potential low cost due to the abundance of the active materials, low toxicity and relative safety,[3] make them an attractive energy storage solution for a wide variety of applications, such as space exploration[4] and low temperature energy delivery.[5] However, the relatively low power capabilities, significant self discharge and low cycle life have so far hindered mainstream adoption of LiS cells. Degradation mechanisms such as lithium anode corrosion, self discharge and low coulombic efficiency have all been related to the polysulfide shuttle. As a result, most effort in the research community is currently directed toward decreasing the amount of shuttle through material design, and assessing the properties of the proposed materials through coin cell characterization.

We argue that equally important for accelerating the adoption of this battery chemistry is the understanding of how real cells behave under real operating conditions, which often include incomplete charge/discharge cycles, noisy current loads and rest periods at various states of charge (SoC). Understanding and detecting the mechanisms leading to degradation, such as capacity fade, are intermediate steps crucial to predicting cycle life. Such understanding can help harvest the most from a given LiS cell, by informing the tuning of operation conditions, within the range allowed by a particular application, to achieve optimum performance.

Experimental studies into the effect of varying the voltage window and current rate provide some indication of the factors limiting cycle life. Degradation of cell performance is generally observed for procedures that allow the cell to be in high or low voltage ranges. Avoiding these regions has been successful at increasing cycle life, such as by limiting the operation to the low voltage plateau, and thus using only 75% of the cell capacity.[6] At the higher end of the voltage range, the oxidation of polysulfides in reaction with the electrolyte, enhanced by the presence of shuttle, has been hypothesized as the main cause of capacity fade.[7] The additive often used as a shuttle suppressant, $LiNO_3$, was found to not alleviate this problem permanently, as it is consumed by oxidative reaction with polysulfides, thus contributing itself to capacity fade. At the lower end of the voltage range, the slow dissolution of the precipitated low order polysulfides was shown to limit cycling performance.[8] The presence of this bottleneck and its effect during a constant current charge have also been predicted by and analyzed via a zero dimensional model of the LiS cathode.[9] The same effect, i.e. the accumulation of a non-conductive film of insoluble Li_2S_2/Li_2S, was shown to be correlated to the largest capacity fade, from amongst three possible causes.[10] Discharging below 1.8 V was shown to greatly accelerate degradation in coin cells with catholyte and shuttle suppressant, effect interpreted to be the result of producing poorly reversible Li_2S from Li_2S_2.[11] Most of these studies, however, are performed on coin cells with excess electrolyte and low electrode loading, which were shown to have markedly different capacity fade rate and mechanism[12,13] compared to a commercially viable cell.[14]

The effect of previous cycles on the present performance of the LiS cell can be strong and determining in applications; however, it has received little attention. It was found that performance is affected by the order in which the cycling rate is varied and by whether both the charge and discharge rates are varied.[15] The results of this comprehensive study also indicate that there is a reversible and an irreversible contribution to capacity fade, since long-term and short term cycling data can indicate opposing cycling procedures and cell compositions as optima. They conclude that a 'medium' charging rate is the best compromise between limiting the overpotential due to Li_2S oxidation and minimizing shuttle.

These results highlight the need for a validated model that can aid in exploring the large number of combinations of operating conditions, from which an optimum must be found. Increasing the cycle life, such as by reducing the voltage window, usually comes at the cost of reduced energy throughput per cycle. But under which operation mode is the energy throughput per cell life maximized? Currently, there is no available tool to quantitatively inform such decisions, and only few degradation-aware models for LiS have been published. A

[z]E-mail: monica.marinescu@imperial.ac.uk

probability-based mathematical model was proposed for discharge, and reproduced capacity fade of coin LiS cells.[16] This model, however, does not address the physical phenomena that cause the fade. Two physical models have been used for predicting cycling behavior. The one dimensional model developed by Hofmann et al. includes shuttle as a reaction occurring at the anode, and thus predicts Coulombic inefficiency.[17] Also at the anode, lithium sulfide can precipitate and accumulate, thus leading to capacity fade with cycling. The 1D+1D model proposed by Danner et al. describes a cell with polysulfides confined by carbon particles in the cathode.[18] In their model, an irreversible loss of active material occurs as a result of S^{2-} ions escaping the cathode confinement, which occurs especially when a high solubility of Li_2S is assumed. A comparison to experimental data for validation is not included with either model.

Both physical degradation-aware models are one dimensional. One dimensional models generally suffer from a number of drawbacks, making them, at least for now, unsuitable for assessing battery performance either in applications, or as a basis for identification and control algorithms. They include a large number of parameters, with values not readily available, are difficult to parameterize and computationally costly, making them unsuitable for simulating cell behavior over many cycles. Zero dimensional models have the potential to become the ideal platform for cycle life studies, due to three essential features. They were shown to capture many of the relevant features of LiS behavior during both charge and discharge, require relatively short computational times, and depend on relatively few parameters, allowing tractability of all included mechanisms.[9] Here, we further develop a previously proposed zero-dimensional physical model, with the aim to develop a quantitative tool for improving the cycle life performance of LiS cells by informing the optimal cycling conditions. The model predictions are validated against experimental data of pouch cells with competitive performance characteristics.

In this work we illustrate that cycling a LiS cell within a limited SoC window, i.e. capacity-limited partial cycling, leads to gradual SoC and voltage drift, thus accelerating the apparent aging rate of the cell. The observed behavior can be predicted by a zero dimensional model that includes a simple mechanism of two electrochemical reactions, kinetic limitations, and precipitation/dissolution of one reaction product. It is shown that shuttle and dissolution rates together dictate the cell behavior under cycling. Shuttle-related degradation via loss of active material is required to reproduce the apparent cell death observed in experiments. The apparent capacity, as measured from the current throughput, is shown to be an extremely poor measure of the cell SoC; instead, the available and dormant capacities predicted by the model should be used instead for state of charge estimation. Based on the understanding gained from model simulations, we are able to propose an approach to increasing cycle life.

Experimental Results and Discussion

Partial cycling experiments were performed on 3.4 Ah cells manufactured by OXIS Energy Ltd. The cells contain a sulfone-based solvent and their electrolyte/sulfur ratio has been optimized in order to deliver maximum cell-level specific energy density, thus indicating a relatively high sulfur and low electrolyte loading compared to the cells in most other published results. In order to emulate their use in an application where a fixed amount of energy is required each time, the charge throughput for charge and discharge was limited at 1.02Ah, calculated by coulomb counting ($Q = I \cdot t$) and corresponding to 30 % SoC. Additionally, safety voltage cutoffs were set at 1.5 V and 2.45 V. Before cycling, cells were charged at 0.1C (0.34 A) to 2.45 V, and then discharged at 0.2C (0.68 A) by 0%, 35% (1.2 Ah) or 70% (2.4 Ah) of the nominal capacity, to correspond to cycling starting from fully charged, two thirds charged and one third charged.

The voltage and charge throughput (in Ah) during cycling of a cell at 0.3C charge/0.3C discharge (1.02 A/1.02 A) starting from fully charged are illustrated in Figure 1. For clarity, only the final voltage of every charge and discharge is plotted; this subset of values is called from here on the voltage envelope. The most apparent feature

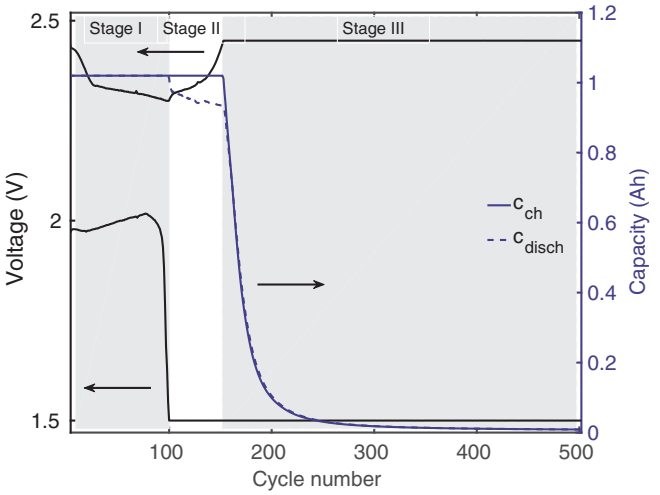

Figure 1. Experimental data: The voltage and capacity of a cell during partial cycling decrease gradually, giving rise to three stages. A fully charged 3.4 Ah cell manufactured by Oxis Ltd. is discharged/charged for 3600 s/3600 s at 0.3C/0.3C. Additional voltage cutoffs are set at 1.5 V/2.45 V. For clarity, only the final voltage of every charge and discharge is plotted, forming the so-called *voltage envelope*. The capacity during charge and discharge is calculated as coulomb-counted charge throughput.

of the voltage envelope is the voltage drift: despite seeing the same charge throughput during charge and discharge, the cell voltage hits the lower and then the higher voltage cutoff. Once the latter occurs, a sharp decrease in charge throughput leads to apparent cell death. Figure 2 illustrates charge and discharge voltage curves of sample cycles belonging to each of the three identified stages.

Stage I is characterized by a narrowing of the voltage envelope: the upper voltage decreases while the lower voltage increases. Charge and discharge capacities, as measured by charge throughput, are equal and constant, illustrating the fact that both charge and discharge can occur for the pre-set time, without causing the cell to reach either voltage cutoff. The discharge voltage curves for cycles number 3 and 4 in Figure 2 indicate that the capacity delivered in the high

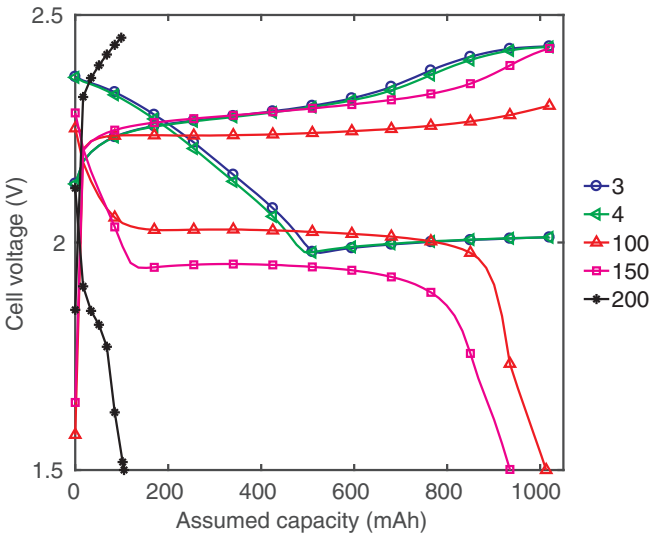

Figure 2. Experimental data: Voltage curves corresponding to discharge and the following charge show a voltage and capacity decrease during the partial cycling procedure. Firstly, the discharge capacity of the high plateau decreases, followed by that of the low plateau. The numbers in the legend correspond to the same cycle number on the x-axis of Figure 1.

plateau is quickly and significantly reduced, leading to a drift in the average voltage during discharge. Whether this drift is an effect of the shuttle, of the dissolution bottleneck, or of another cause, cannot be ascertained without further investigation, and is discussed in the Model predictions without degradation section and Model predictions with degradation section. The drift is also visible during charging, during which the higher plateau is reached progressively later within the SoC window.

Stage II begins once the lower cutoff voltage is reached; now the upper voltage increases with every charge. The charge capacity remains constant, while the discharge capacity decreases with every cycle. Discharge occurs for increasingly shorter time durations because the lower voltage cutoff is reached sooner. Importantly, the difference between charge and discharge capacities should not be interpreted as charging inefficiency due to shuttle; losses due to shuttle exist, but cannot be identified directly from this data, because the cycling procedure fixes the charge throughput. Cycles number 100 and 150 happen to correspond to the beginning and end of stage II; the cell voltage during these two cycles is plotted in Figure 2. In stage II, the decrease in discharge capacity comes solely from a decrease in the capacity of the lower plateau. The plateau voltage is considerably lower at the end of stage II, indicating a significantly increased cell resistance. The charge at the beginning of this stage shows behavior consistent with that in stage I, namely an increase in the amount of time spent in the lower plateau compared to the first cycles. At the end of stage II, however, charging reaches again the higher plateau. It is difficult to ascertain the cause of these features.

Stage III begins once the higher voltage cutoff is reached. Cycling has become limited by the two voltage cutoffs. Charge and discharge capacities decrease because the time to reach the voltage cutoff decreases abruptly from one cycle to the next. The discharge capacity is slightly higher than the charge capacity during most of stage III. The cause for this difference has not been explored.

The presence of the three stages in the partial cycling behavior remains consistent during the following variations to the standard cycling conditions described above. Plots of the corresponding experimental data are included in Supplementary material A.

Initial capacity. When the cell is cycled starting from a more discharged state, the total number of cycles before the apparent cell death is smaller. Cells starting the procedure fully charged cycle for longer than those starting from 65% SoC, and similarly for 65% vs 30%, as illustrated in Figure 1 in Supplementary material A. The difference in cycle life is almost solely due to a decrease in stage one.

Current rate for both charge and discharge. Decreasing the current rate for both charge and discharge to 0.15C greatly increases cycling life, shown in Figure 2 in Supplementary material A. In this case, stages I and II, measured in cycle numbers, are significantly longer.

Upper voltage cutoff. Decreasing the upper voltage cutoff limit to 2.33V greatly increases cycle life, due to an increase in the number of cycles in stage I, possibly due to limiting the effect of shuttle, shown in Figure 3 of Supplementary material A. Only stage I and II appear, because the low upper voltage limits the voltage increase.

Conclusions from experimental data.—The voltage drift followed by a decay of charge throughput per cycle are the main features of the cell behavior, both with important implications for applications. During stage III, discharges belonging to various cycle numbers start from the same voltage but yield starkly different capacities, illustrating a strong effect of cycling history on current performance. Understanding and tracking the effects of this history effect are essential not only for ensuring reproducibility of data, but also for designing robust estimation and control algorithms. Because of a mostly flat voltage plateau during discharge and of shuttle during charge, coulomb counting and voltage-reading are both ineffective, leaving no direct experimental tool for the identification of the LiS SoC.[19]

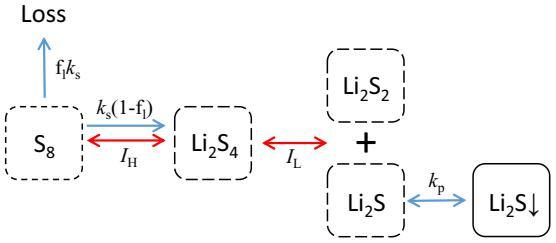

Figure 3. Schematic of the model: The current at the cell terminals is the sum of the currents of the two electrochemical reactions occuring in parallel. High order polysulfides (S_8^0) convert to middle order polysulfides (S_4^{2-}) also in the absence of current, as a result of the polysulfide shuttle. A fraction of the shuttled material is lost irreversibly. Part of the final product (S^{2-}) precipitates/dissolves according to a precipitation constant.

The voltage drift is expected to be the result of shuttle and incomplete dissolution. The effect of slow dissolution is expected to be weaker for lower charging currents, thus explaining the overall positive effect of using low-rate currents. Many of the more detailed features of the cell's response to the cycling procedure, however, cannot be explained from this data alone. The main features requiring further exploration are listed below.

1. As the voltage decreases in stage I, the effect of shuttle is expected to decrease. What causes the increase in the upper value of the voltage envelope during stage II in Figure 1?
2. The cause of the abrupt decrease in charge throughput in stage III is not clear (Figure 1).
3. The transition between low and high plateau during charge seems to move to later times and then back to earlier times during the cycling procedure, as visible in Figure 2. Why?
4. In stage I the high plateau capacity becomes lower, while during stage II the low plateau capacity decreases. What causes this?

We conclude that a model is required to track the true capacity of the cell, the current lost through shuttle, and the quantity of undissolved precipitate throughout cycling. Such a model should be able to differentiate between irreversible and reversible capacity loss, and could be used as a tool for designing optimum procedures for capacity recovery.

Model

The proposed model is an improvement to the zero-dimensional electrochemical model of a LiS cathode published by Marinescu et al., which was shown to reproduce main LiS cell characteristics during charge and discharge.[9] Below, the complete set of equations is summarized, while Figure 3 illustrates a schematic of the various mechanisms included. A description of the variables and parameters used, together with their values, is given in Table I.

The model assumes that a single electrochemical reaction dominates each of the two discharge regions. The two reactions allowed in the system are

$$S_8^0 + 4e^- \leftrightarrow 2S_4^{2-}, \qquad [1a]$$

$$S_4^{2-} + 4e^- \leftrightarrow 2S^{2-} \downarrow + S_2^{2-}, \qquad [1b]$$

and take place during both discharge and charge. This reaction mechanism corresponds to that chosen by Mikhaylik and Akridge[22] and represents the simplest reaction mechanism that includes both precipitating and non-precipitating final discharge products.

When fully charged, the sulfur in the cell is assumed to be mostly in the form of S_8^0, a dissolved species. Because the upper voltage limit

Table I. Values of model parameters. Subscripts 'H' and 'L' denote quantities relevant to the reactions in Equation 1a and 1b respectively, generally determining the high and low voltage plateaus.

Notation	Name	Units	Value
Physical constants			
F	Faraday constant	C mol^{-1}	9.649×10^4
M_S	molar mass of S_8^0	g mol^{-1}	32
N_A	Avogadro number	mol^{-1}	6.0221×10^{23}
n_4	electron number per reaction	-	4
$n_{S8}, n_{S4}, n_{S2}, n_S$	number of S atoms in polysulfide	-	8, 4, 2, 1
R	gas constant	J K^{-1}mol^{-1}	8.3145
ρ_S	density of precipitated sulfur	g L^{-1}	2×10^3
Cell design properties, assumed as in Marinescu et al.[9]			
a_r	active reaction area per cell	m^2	0.960
f_H	dimensionality factor H	g L mol^{-1}	0.7296
f_L	dimensionality factor L	g^{2}L^2 mol^{-1}	0.0665
v	electrolyte volume per cell	L	0.0114
m_S	mass of active sulfur per cell	g	2.7
Kinetic properties			
E_H^0	standard potential H	V	2.35
E_L^0	standard potential L	V	2.18
$i_{H,0}$	exchange current density H	A m^{-2}	1
$i_{L,0}$	exchange current density L	A m^{-2}	0.5
Shuttle and precipitation parameters			
S_*^{2-}	S^{2-} saturation mass	g	5×10^{-5}
k_p	precipitation rate	s^{-1}	100
k_s	shuttle constant	s^{-1}	charge: var, disch: 0
f_s	loss rate due to shuttle	-	0.25
Operational parameters			
I	external current	A	discharge: I>0, charge: I<0
T	temperature	°K	298
Variables			
E_H, E_L	Nernst potentials	V	
i_H, i_L	current contributions	A	
η_H, η_L	overpotentials	V	
V_c	cathode voltage	V	
S_8^0, S_4^{2-}, S^{2-}	mass of dissolved sulfur	g	
S_p	mass of precipitated S^{2-}	g	
S_s	mass of shuttled sulfur	g	
S_l	mass of lost sulfur	g	
Auxiliary variables			
c_{th}	theoretical capacity	Ah	

is set to 2.45V, it is expected no significant quantities of solid S_8 are formed. The theoretical capacity of the cell c_{th}, corresponding to the true SoC, is given by

$$c_{th}[Ah] = \left(\frac{3n_4}{n_{S8}}\frac{F}{M_S}S_8^0 + \frac{n_4}{n_{S4}}\frac{F}{M_S}S_4^{2-}\right)\frac{1000}{3600}, \quad [2]$$

where $n_4 = 4$ represents the number of electrons contributed by each of the two reactions in Equation 1, n_{S8}, n_{S4} the number of sulfur atoms in each polysulfide, S_8^0, S_4^{2-} the amounts of sulfur dissolved in the electrolyte in the respective form in grams, F the Faraday constant, and M_S the molar mass of sulfur. Each S_8^0 molecule contributes twelve electrons to the capacity of the cell, and each S_4^{2-} four electrons. The value of the true instantaneous cell capacity can be markedly different from the capacity assumed by coulomb counting, which remains constant from one cycle to another, for the partial cycling procedure used here. The expression in Equation 2 is valid only for the reaction path chosen in the model, as given in Equation 1.

The equilibrium potential for the two reactions is assumed to obey the Nernst equation

$$E_H = E_H^0 + \frac{RT}{n_4F}\ln\left(f_H\frac{S_8^0}{(S_4^{2-})^2}\right), \quad [3a]$$

$$E_L = E_L^0 + \frac{RT}{n_4F}\ln\left(f_L\frac{S_4^{2-}}{(S^{2-})^2 S_2^{2-}}\right), \quad [3b]$$

where E_H^0, E_L^0 are the standard potentials for Equation 1a and 1b respectively, R is the gas constant, and T the temperature. The factors f_L, f_H ensure that species quantities measured in grams are compatible with the Nernst formulation in Equation 3:

$$f_H = \frac{n_{S4}^2 M_S v}{n_{S8}}, \quad [4a]$$

$$f_L = \frac{n_S^2 n_{S2} M_S^2 v^2}{n_{S4}}, \quad [4b]$$

where v is the volume of electrolyte in the system. The total current through the battery is given as the sum of currents for the two reactions

$$I = i_H + i_L. \quad [5]$$

The currents associated with the two reactions are described by the Butler-Volmer approximation:

$$i_H = -2i_{H,0}a_r \sinh\frac{n_4F\eta_H}{2RT}, \quad [6a]$$

$$i_L = -2i_{L,0}a_r \sinh\frac{n_4F\eta_L}{2RT}, \quad [6b]$$

where $i_{H,0}, i_{L,0}$ are the exchange current densities, η_H, η_L the surface overpotentials, and a_r the constant active surface area available for the high (H) and low (L) plateau reactions. The overpotential of each reaction is given by

$$\eta_H = V_c - E_H \quad [7a]$$

$$\eta_L = V_c - E_L, \quad [7b]$$

where V_c is the cathode voltage, here assume to equal the measured cell voltage.

The various polysulfide species evolve with time as a result of being produced or consummed by the two electrochemical reactions, the shuttle reaction and the precipitation/dissolution reactions:

$$\frac{dS_8^0}{dt} = -\frac{n_{S8}M_S}{n_4F}i_H - k_s S_8^0 \quad [8a]$$

$$\frac{dS_4^{2-}}{dt} = 2\frac{n_{S4}M_S}{n_4F}i_H + \left(1 - \frac{f_s}{m_S}S_s\right)k_s S_8^0 - \frac{n_{S4}M_S}{n_4F}i_L \quad [8b]$$

$$\frac{dS_2^{2-}}{dt} = \frac{n_{S2}M_S}{n_4F}i_L \quad [8c]$$

$$\frac{dS^{2-}}{dt} = 2\frac{n_S M_S}{n_4F}i_L - \frac{1}{v\rho_S}k_p S_p\left(S^{2-} - S_*^{2-}\right) \quad [8d]$$

$$\frac{dS_p}{dt} = \frac{1}{v\rho_S}k_p S_p\left(S^{2-} - S_*^{2-}\right) \quad [8e]$$

$$\frac{dS_s}{dt} = k_s S_8^0, \quad [8f]$$

where S_p is the mass of precipitated sulfur, ρ_S its density, and S_*^{2-} the saturation mass of S^{2-}, assumed to be constant. With the exception of the degradation term in Equation 8b, which is discussed in Degradation model section, these are the equations used in Marinescu et al.[9]

Degradation model.—The model developed by Marinescu et al.,[9] which does not include a degradation mechanism, cannot retrieve all features of the experimental data, as discussed in the Model predictions without degradation section. We therefore introduce a degradation mechanism, by allowing a fraction of the shuttled polysulfide to become permanently inactive. This mechanism leads to capacity fade and allows the model to capture more of the features observed experimentally. The rate of lost sulfur S_l is defined by the term $\left(-\frac{f_s}{m_S}S_s k_s S_8^0\right)$ in Equation 8b:

$$\frac{dS_l}{dt} = \frac{f_s}{m_S}S_s k_s S_8^0, \quad [9]$$

where the dimensionless loss rate f_s is a positive constant, with $f_s = 0$ leading to no loss. Through this term, an amount of the shuttled S_8^0 does not convert to S_4^{2-}, but is instead lost. The expression for S_l assumes that the fraction of the shuttled material that is rendered inactive, $\frac{f_s}{m_S}S_s$, is proportional to the amount already shuttled, thus increasing as the cell ages further. This concept reflects one possible shuttle-related degradation mechanism: the shuttle reaction leads to a layer of precipitated products at the anode,[20] increasing the anode roughness, and thus providing an increased surface area for further reactions to take place.[21] In practice, this zero dimensional model captures an effective sulfur loss, irrespective of the location where this loss would occur in the real system. The total mass of lost sulfur at a given time can be obtained by integrating Equation 9, with the shuttled sulfur S_s substituted from Equation 8f:

$$S_l(t) = \frac{f_s}{m_S}k_s^2\int_{t_0}^{t}\left(dt\,S_8^0\int_{t_0}^{t}dt\,S_8^0\right) + S_l(t_0). \quad [10]$$

In the current model, the shuttle and any associated degradation are considered to take place only during charge. While self discharge mechanisms do take place during rest, and have been associated with the polysulfide shuttle,[22,23] the relation between the shuttle during cycling and the self discharge during rest is not established. The purpose of this model is to simulate cycling behavior, and so self discharge during storage is not relevant, because no significant time is spent at rest. The presence of shuttle during discharge, its magnitude relative to that during charge, and an associated loss mechanism are much less documented in the literature. For simplicity, the effect of polysulfide shuttle during discharge is ignored in the following analysis.

Other degradation mechanisms have been identified experimentally, both related to and independent from shuttle. In particular, electrolyte depletion and lithium consumption are also expected to play a role in the cycle life of LiS batteries.[24] Developing a model to account for these effects remains the subject of further studies.

Model limitations.—In its current form, the model developed here cannot be used for quantitative prediction, because it does not reproduce the values of the discharge voltage plateaus seen in experiments. The values of E_H^0 and E_L^0 determine the elevation of the plateaus, and can be chosen further apart from one another, thus bringing them closer to the experimentally observed values. This, however, introduces a high computational cost, which is not justified yet in this model.

Perfectly fitting the predicted voltage curves to experimental data cannot yet be a target, as this model predicts only the voltage of the cathode, not of the whole cell. The Ohmic drop contributes significantly to the cell voltage,[25] and varies considerably during discharge. Thus the voltage drop due to the series resistance of the cell, as well as the anode potential, must be considered before fitting to experimental data.

Finally, the model cannot retrieve the diminished capacity obtained with increasing discharge rate. Mass transport limitations, which are not accounted for in this zero dimensional model, have been shown to limit the power rate.[26] The effect of cathode passivation by the insulating precipitate Li_2S at low states of charge, which has been associated with increased overpotential at the beginning of charging,[27] is also disregarded here. It should be noted, however, that Zhang et al. have shown that this effect can be attributed instead to transport limited reaction kinetics.[28] Retrieving the correct rate limitation during discharge remains the subject of future work. In the present study, the focus is placed on using the model as a tool to gather information on the mechanisms behind the observed cycling behavior.

Computational implementation and initial conditions.—Equations 3–8 form a differential algebraic system that can be solved for the thirteen unknowns: the Nernst potentials E_H, E_L, the currents from the two reactions i_H, i_L, the cell voltage V_c, here equal to the cathode voltage, the overpotentials η_H, η_L, the mass of the five forms of sulfur S_8^0, S_4^{2-}, S_2^{2-}, S^{2-}, S_p, and that of the total shuttled sulfur S_s. The Jacobian for the system is calculated analytically and the system is solved in Matlab using a second order solver. For the Matlab code please see Supplementary material B.

Changes in the initial operating conditions, such as the magnitude of the current, were found to lead to non-physical variations in the total sulfur mass in the system (eg. 3%).[9] This error occurred due to the way in which the initial conditions were calculated. For example, in the case of discharge from fully charged, initial values of V_c, S_8^0 and S_p were assumed, η_H was calculated from 6a, under the assumption $I = i_H$, and was thus dependent on I. E_H was calculated from 7a, and S_4^{2-} was then obtained through 3a, and was thus dependent on I. While such small differences in total sulfur mass do not affect the conclusions from the model results, they could become significant once a concentration-dependent series resistance is introduced, as recommended by Zhang et al.[25] Generally, voltage and current should not both be inputs to the model.

Ideally, the initial conditions are obtained by solving the system of equations formed by Equation 3, $E_H = E_L$ and mass conservation. Instead of solving a system with transcendental equations, an alternative procedure is used that ensures systems starting at different operational conditions are perfectly comparable.

For discharge from equilibrium, the initial state of the cell is calculated by assuming the quantities of S_8^0, S_4^{2-} (eg. 998:1 for a charged

cell) and calculating the other polysulfide amounts under conditions of zero current and equilibrium of the precipitation reaction. The former condition imposes $\eta_H = \eta_L = 0$, and thus $V_c = E_H = E_L$, while the latter sets the value of S^{2-} to S_*^{2-}. The model is then run while linearly ramping the current across a short amount of time (0.1 s), from zero to the desired initial discharge rate. For charging from equilibrium, the state of a cell is calculated by running the model on a cell discharged at 0.1C, left to equilibrate against electrochemical reactions and precipitation/dissolution under zero current, and then charged with a brief (0.1s) linear ramping up of the current to the desired initial instantaneous charging current.

Model Results and Discussion

Model parameters.—The system parameters and their default values are given in Table I, where the subscript H denotes the high plateau reaction in Equation 1a and L the low plateau reaction in Equation 1b.

Model predictions without degradation.—Model predictions for a 3.4 Ah cell without degradation are illustrated in Figure 4. Stage I exhibits similar features as the experimental data in Figure 1; the voltage drifts downward, while the charge and discharge capacities are constant and equal. Despite a voltage drift being present, only two stages are visible in Figure 4a. The corresponding evolution of the mass of precipitate S_p and that of the shuttled sulfur are shown for each cycle in Figure 4b. The mass of precipitated sulfur increases during stage I, while the shuttling amount decreases. During stage II, an equilibrium is reached between the input current and the losses through shuttle. It can be seen that, although the shuttle decreases as a result of the voltage drift, it never becomes zero.

The model predicts a voltage drift as the combined consequence of precipitate accumulation and charging inefficiency due to shuttle.

- The upper voltage decreases as a direct result of shuttle: during each charge a fraction of the input energy is lost through shuttle, while each discharge still occurs for the pre-specified 30% SoC. The usable capacity of the cell (Equation 2) at the end of a charge decreases, as illustrated in Figure 4c, and so does the maximum voltage reached.
- The significant decrease in the lower voltage, however, is a direct consequence of two mechanisms: firstly, according to this model, S^{2-} precipitates more readily than it dissolves, as explained below, and secondly the rate of the electrochemical reactions during charging is limited by the amount of Li_2S that dissolves. This phenomenon will be referred to as the *dissolution bottleneck*. If the precipitation and dissolution processes were symmetrical, the lower voltage would remain constant, initially due to the fact that it is tracing the voltage of the lower plateau of a constant current discharge. Once the drift brought the cell to a low enough SoC, the shuttle impact would be diminished, and no further drift would occur. This can be verified by running the model with shuttle but no precipitation, such as by setting a high saturation concentration, which yields the voltage behavior presented in Figure 5a, with shuttled mass given in Figure 5b; without a dissolution bottleneck, stage I becomes infinite. The dissolution bottleneck, associated here with the precipitating species S^{2-}, renders part of the active sulfur temporarily unusable, and thus decreases the cell capacity with every cycle. The voltage drift occurs faster than in the case of no precipitation, as the lower limit of the voltage envelope moves along a constant current discharge curve of ever increasing current rate. This effective increase in the current rate leads to the lower voltage cutoff being reached significantly faster in a model with precipitation and no shuttle, Figure 5c, than in the one without precipitation, Figure 5a.

The model is highly sensitive to the value of S_*^{2-}, which determines whether the amount of precipitate increases with cycling, or reaches a dynamic equilibrium; the behavior of the two types of cells is shown in Figure 5d.

The voltage curves predicted by the model with both shuttle and precipitation during selected cycles are illustrated in Figure 4d and are similar to the experimental data in Figure 2. The discharge capacity in the high voltage plateau decreases, followed by that of the low voltage plateau, consistent with a drift in cell SoC. While the cell remains within the higher plateau during the first cycle, it enters the lower plateau already in the second cycle, because the charge in-between the two discharges is not complete, as a result of shuttle. Once the cell spends significant time in the lower plateau, precipitate starts to accumulate, and the usable capacity of the cell decreases. Charging inefficiency and reduced cell capacity both act to lower the average cell SoC from one cycle to the next.

The lower voltage cutoff is reached when the cell is fully discharged, corresponding to half the sulfur being in the form of S^{2-} or S_p, as the maximum quantity of precipitate allowed by the assumed reaction mechanism. Further cycling repeats identically, as a dynamic equilibrium has been reached: the difference between charging and discharging times, or energy throughputs, compensates the effect of shuttle.

Mechanism of precipitate accumulation.—Precipitate accumulates during cycling because of the form of the precipitation/dissolution term in Equation 8e, and despite the parameters k_p and S_*^{2-} having the same value during charge and discharge. The mechanism of accumulation is visible in Figures 4e and 4f:

- The average cell capacity decreases with cycling, and reaches progressively deeper into the lower plateau, allowing for precipitation to start occurring earlier in the discharge cycle;
- The amount precipitated per unit time is significantly higher than the amount subsequently dissolved, due to the relation used for precipitation/dissolution.[29] The term $(S^{2-} - S_*^{2-})$ in Equation 8e allows infinite driving force for precipitation, because a higher current drives the electrochemical reaction faster and can build a supersaturated solution. On the contrary, the dissolution rate during charge is limited by $0 < S^{2-} < S_*^{2-}$;
- While precipitation stops as soon as the current changes from discharge to charge, dissolution can continue during the discharge, effectively providing a reservoir of active material with its own response time;
- With further cycling, as more sulfur is trapped as precipitate, a large driving force for precipitation is more difficult to achieve, and the rates of dissolution and precipitation become comparable.

The presence of a third stage, as seen in the experimental data, is retrieved only by the model with loss.

*The disappearance of the voltage dip within the first few discharges.—*The disappearance of the dip within the first few cycles, visible in Figure 2 and in Figure 4e, can be understood by analyzing in more detail the model predictions for the first five cycles. The evolution of species, shown in Figure 6a, confirms the capacity drift conclusion - in effect, the capacity window of operation shifts toward lower capacities from one cycle to another. The precipitated S_p increases and the interval of values taken by S_4^{2-} shifts slowly past the 'mountain peak' associated with the boundary between plateaus. Figure 6b illustrates the evolution of the cell voltage, while Figure 6c illustrates the corresponding S^{2-} evolution during the same first five cycles. The model predicts that a pronounced dip quickly becomes shallower within the first few cycles. In the model, the voltage dip appears if the electrolyte is supersaturated with S^{2-}. This state cannot occur once precipitate has accumulated, because the total mass of dissolved S^{2-} is smaller and the rate of precipitation increases proportional to the amount of already precipitated material. The dip in-between the two voltage plateaus is a feature often but not always seen in the literature. In the experiments presented here, the dip is not as visible as predicted by the model, most probably because the cells have been pre-cycled.

Model predictions with degradation.—Predictions of the model that includes a loss of active material through shuttle are illustrated

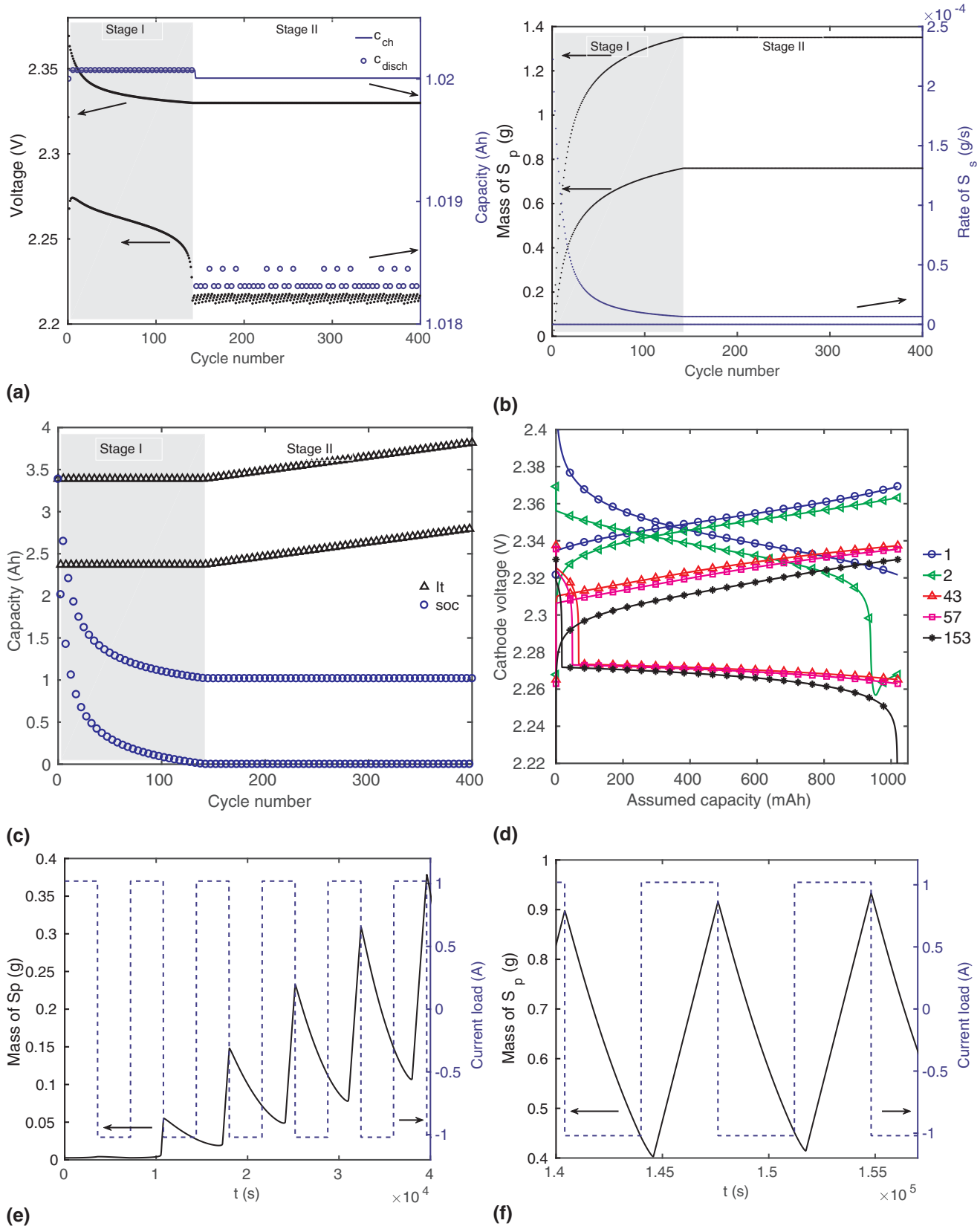

Figure 4. Model predictions without degradation: the SoC drifts due to shuttle and precipitation accumulation, and stabilizes once the cell is fully discharged and shuttle is mostly avoided. For a 3.4 Ah cell cycled at 0.3C/0.3C charge/discharge from fully charged for 3600 s/3600 s with a 2.21 V/2.38 V voltage cutoff, without degradation ($f_s = 0$), and $k_s = 10^{-4}s^{-1}$: a) Voltage envelope and associated charge and discharge capacity throughput, calculated from $I \cdot t$; b) amounts of shuttled sulfur and precipitated S^{2-}; c) instantaneous true and assumed capacities of the cell, as calculated from concentrations of available species (soc) and $I \cdot t$ (It) respectively; d) Voltage curves during discharge and the following charge at various points during cycling; e) and f) evolution of precipitated sulfur and the associated applied current during sample cycles ($I < 0$ during charge and $I > 0$ during discharge).

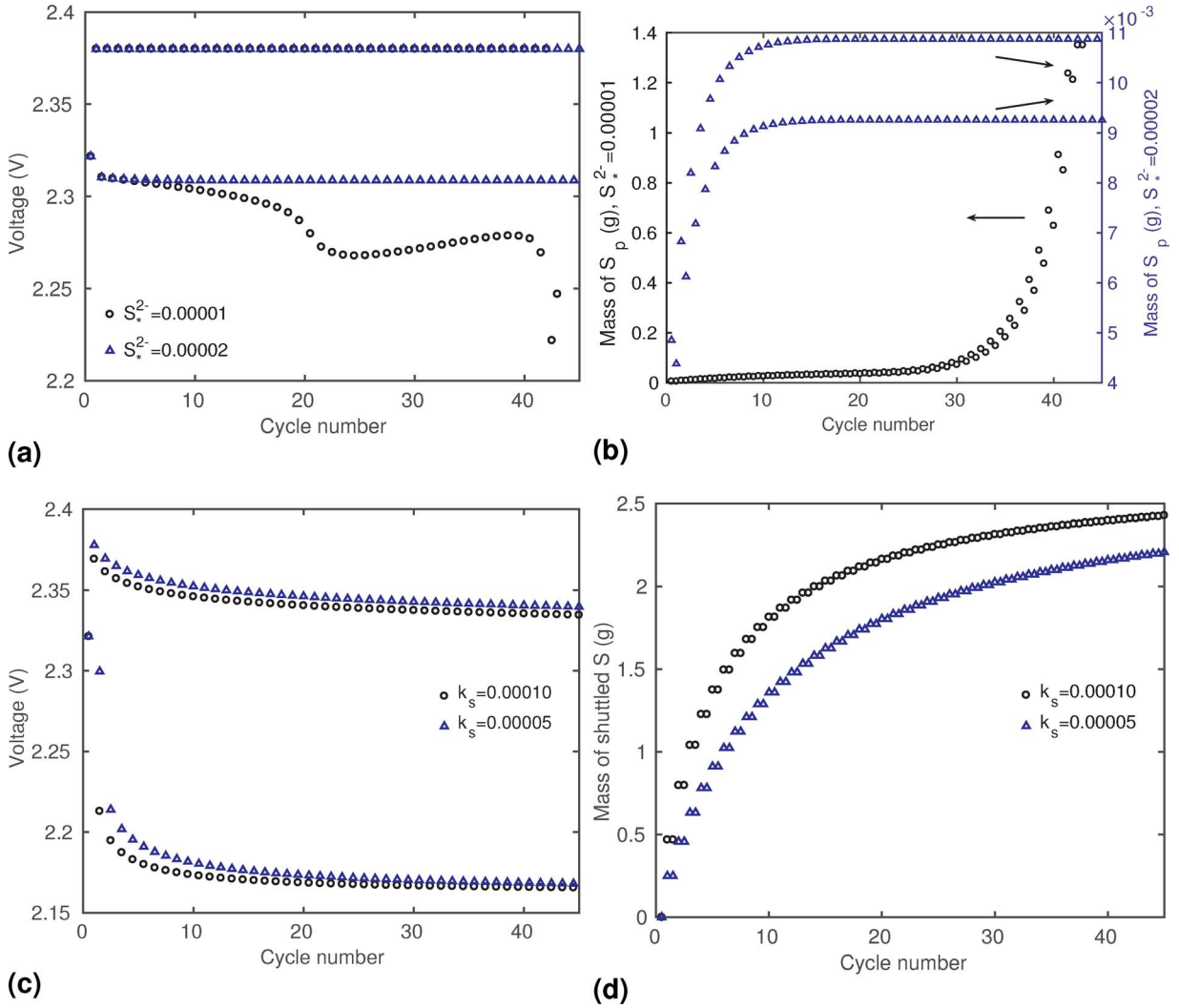

Figure 5. Model predictions: Voltage envelope of a 3.4 Ah cell cycled at 0.3C/0.3C charge/discharge for 3600 s/3600 s from fully charged, without loss ($f_s = 0$), for case (i). only shuttle: $S_*^{2-} = 3$ g such that all sulfur is in a dissolved state a) voltage envelope and b) shuttled mass, and for case (ii). only precipitation: $k_s = 0$, with safety voltage cutoff 2.22/2.38 V c) voltage envelope and d) precipitated mass.

in Figure 7. Figure 7a shows the voltage of the cell exhibits the three stages observed experimentally. The corresponding species evolution is plotted in Figure 7b. As in the case of the model without degradation, illustrated in Figure 4, stage I is characterized by the accumulation of precipitate, and an associated decrease of the average cell SoC and total cell capacity. Once the cell is fully discharged, i.e. the maximum amount is precipitated, the lower voltage cutoff is reached, marking the beginning of stage II. In generating the data for Figure 4 and Figure 7, while all other parameter values remain the same, the shuttle rate is significantly different. Due to degradation, in order for stage I to have a similar length, the value of k_s must be smaller in the case of loss than in the case of no loss.

In this degradation-aware model equilibrium cannot be reached during stage II. Despite relatively minor shuttle, the losses associated with degradation (S_l in Figure 7b) gradually decrease the total capacity of the cell. The fixed charge/discharge current corresponds to increasing C-rate values, allowing the upper voltage to increase without a corresponding increase in the cell capacity at the end of charging. The true cell capacity, as calculated from the availability of dissolved sulfur species, is illustrated in Figure 7c. The dormant capacity corresponds to the amount of S_p that is undissolved at the end of each charge, and thus momentarily unavailable, despite not being lost. The maximum capacity corresponds to the sum of active and dormant capacities in the cell, its decrease with cycle number corresponding to the amount of material lost through shuttling. Both capacities are obtained from the respective masses of sulfur, through the relation

$$[\text{capacity}] = \frac{12}{8}\frac{\text{F}}{\text{M}_\text{S}}\frac{[\text{mass}]}{3600} \qquad [11]$$

where, in this case, the *mass* is either S_p (for dormant capacity), or $(m_S - S_l)$ (for maximum capacity), both at the end of charge. Figure 7c makes it apparent that, during stage II, the cell is cycled between the same true capacity values, while its maximum capacity, given by the mass of sulfur that is not lost, is decreasing. The end of stage II is reached when the cell reaches the higher voltage cutoff when charged with the desired charge throughput. During stage III, there is not enough active capacity left in the cell, as given by the difference between the maximum and dormant capacities. In a model without loss, an increase of the upper voltage envelope can only be reproduced by assuming extremely strong precipitation, which is unrealistic, as it would lead to extremely poor cyclability. Each charge in stage III is voltage-limited, causing the true capacity at the end of each subsequent charge to decrease. The steep decrease in the charge throughput, apparent in Figure 7a, is thus a direct consequence of the voltage-limited cycling coupled with an ever-increasing effective C-rate of the charging current. The latter is indicated by the sharp increase in dormant capacity during stage III i.e. in the amount of

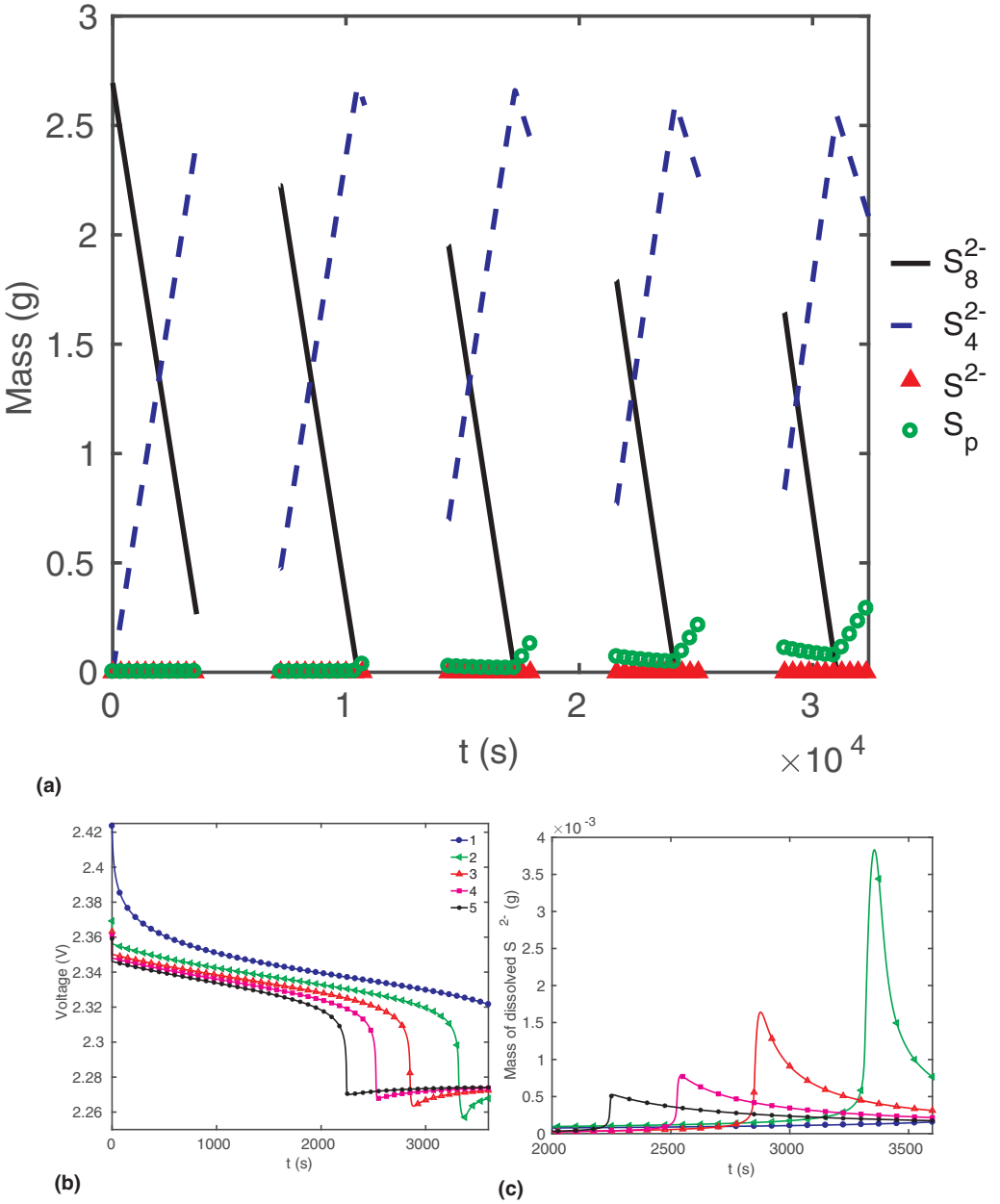

Figure 6. Model predictions: a) Species amounts, b) cell voltage and c) mass of dissolved S^{2-} during the first five cycles of the modeling data in Figure 4. The average cell SoC decreases during cycling, as seen by the increased contribution of the lower plateau reaction to the discharge capacity. The voltage dip in-between the plateaus, initially caused by supersaturation of the electrolyte with S^{2-}, disappears within the first few cycles. As precipitated sulfur accumulates, the conditions for a strong supersaturated state cannot be met.

sulfur that remains precipitated at the end of each charge (also visible in Figure 7b), caused by the decreasing length of the charging half-cycle. Figure 7e and Figure 7f show the same mechanism of precipitate S_p accumulation is occurring here, as in the case of the model without degradation.

The effects leading to reversible and irreversible losses are coupled in this model: the stronger the effect of precipitation, i.e. the more precipitated S_p accumulates, the larger the contribution of the upper plateau reaction to the charging current, the more shuttle, and thus the more sulfur loss and capacity loss. This coupling is a consequence of the assumption made here, that the amount of shuttle is dependent on the amount of S_8^0, and not directly on the cell voltage.

The model with degradation seems to capture the important phenomena playing a role in the cell behavior during partial cycling: the three stages are retrieved due to an increase in the upper voltage during stage II, and the predicted charge and discharge voltages at various cycles in the procedure are qualitatively similar to experimental data, Figure 7d. Both the upper and the lower voltage plateaus become lower with cycling. A lowering of the voltage plateaus has also been retrieved by a one dimensional model proposed by Hofmann et al.,[17] where precipitated Li_2S accumulates with cycling on the anode. Experimentally, a reduced discharge capacity with cycling was linked to an effective increase in charge rates by Poux et al.,[15] who probably witnessed a manifestation of the dissolution bottleneck.

Differences between the shape of the predicted and real voltage envelopes are mainly due to differences between the predicted and real cell voltage during a constant current discharge. These errors are inherent to the use of the relatively simple set of only two electrochemical reactions in the model.

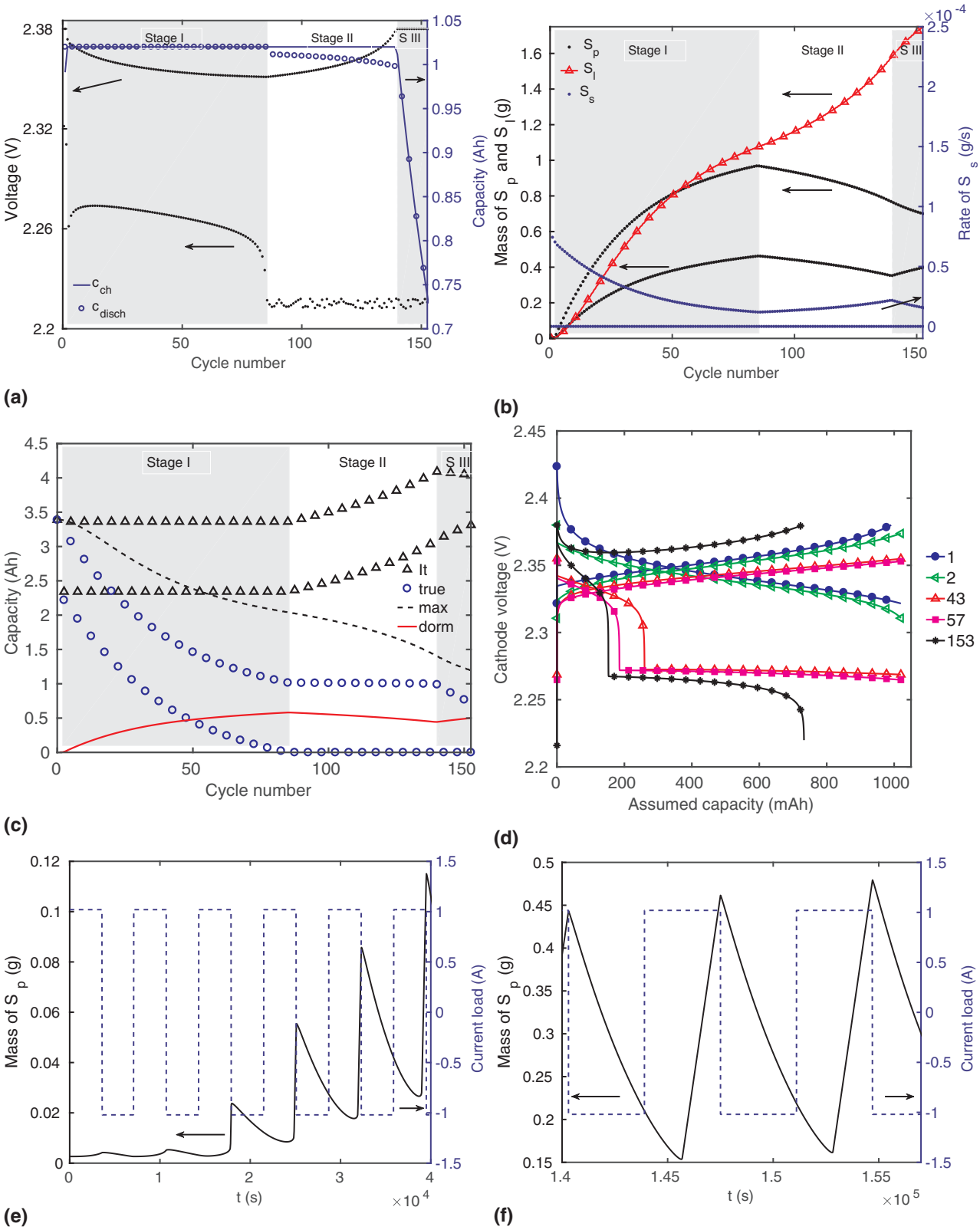

Figure 7. Model predictions with degradation: when assuming sulfur mass is rendered gradually inactive, such as due to shuttle, the three stages of cycling seen in the experimental data in Figure 1 can be retrieved. For a 3.4 Ah cell cycled at 0.3C/0.3C charge/discharge from fully charged for 3600 s/3600 s with a 2.21 V/2.38 V voltage cutoff, with degradation $f_s = 0.25$, $k_s = 3 \times 10^{-5}$ s^{-1}: a) Voltage envelope and associated charge and discharge capacity throughput, calculated from $I \cdot t$; b) rate of shuttling sulfur, and masses of precipitated and lost sulfur; c) instantaneous assumed and true capacities, as calculated from $I \cdot t$ (It) and concentrations of available species (true) from Equation 2; maximum theoretical capacity (max) corresponding to the mass of sulfur that is not lost through shuttle, and dormant capacity (dorm), corresponding to the amount of precipitate left at the end of each charge; d) voltage curves during discharge and the following charge at various points during cycling; e) and f) evolution of precipitated sulfur and the applied current during sample cycles (I < 0 during charge and I > 0 during discharge).

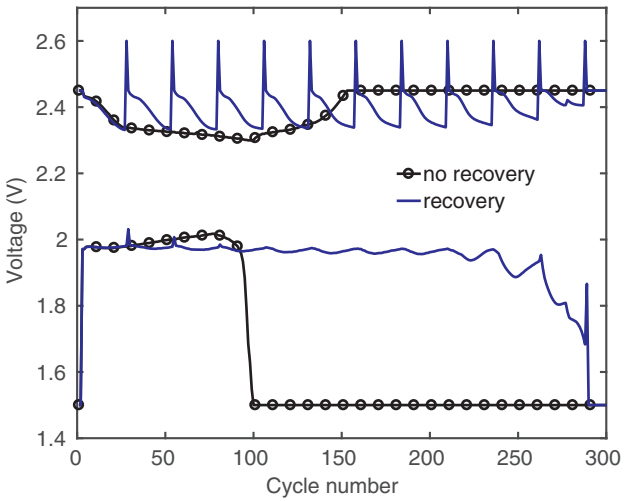

Figure 8. Experimental data: A lower rate charge applied at regular intervals prolongs the cycle life of a cell under partial cycling, but not indefinitely. Both cells are cycled according to the reference procedure of 0.3C/0.3C discharge/charge from fully charged, with additional voltage cutoffs at 1.5 V/2.45 V. One cell undergoes a recovery procedure, being charged at 0.1C instead of 0.3C every 25 cycles.

Crucially, the model predicts that the lost capacity leading to the voltage drift is partially reversible, because it is partially caused by the accumulation of precipitate, active material which is, in theory, only temporarily unavailable. Charging via a lower current rate should recover at least some of this capacity, as it allows more time for the dissolution of S_p to occur. Low current charging, however, is expected to also introduce more irreversible loss, as the cell remains in the shuttling region for longer.

The effect of recovery cycles.—Based on model predictions, a cell identical to that described in Experimental results and discussion section was charged at 0.1C (0.34A) once every 25 cycles (instead of 0.3C), with 2.45 V upper voltage cutoff. The cell response is shown in Figure 8. As expected, the voltage drift is reduced; however, it is not eliminated.

Predictions of a cell's voltage under cycling with periodic recovery via slower charging are illustrated in Figure 9a for the model without loss and in Figure 9b for the model with loss. The model without degradation exaggerates the positive effect of the recovery cycle, while the model with degradation exaggerates its negative effect, compared to the experimentally measured behavior. It can be seen in Figure 9c that the full amount of S_p is dissolved during a recovery cycle in the model without loss, such that, as long as recovery occurs each time before stage I ends, i.e. before the lower voltage cutoff is reached, the procedure can be repeated indefinitely. In the model with degradation,

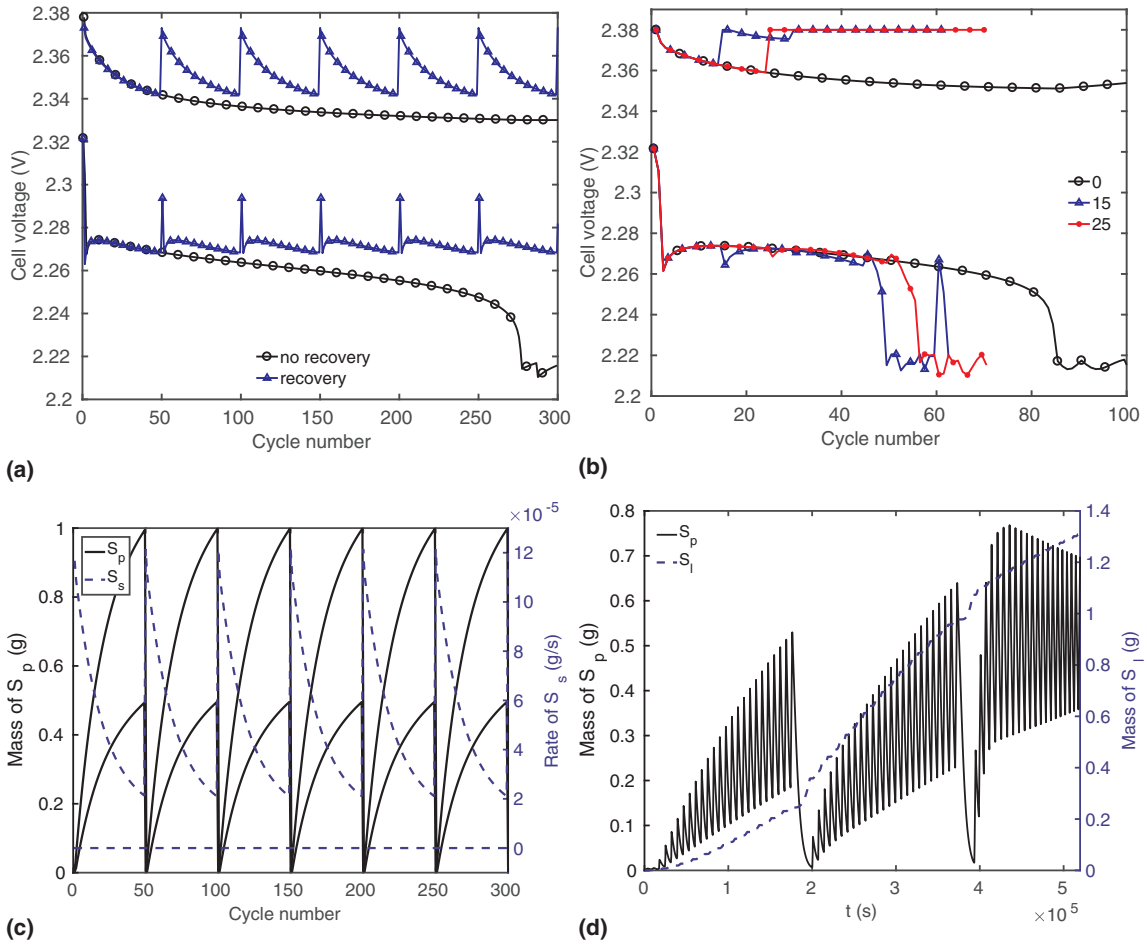

Figure 9. Model predictions: the model without degradation predicts the beneficial effect of a periodic recovery in the form of a slower rate charge, while the model with shuttle-induced capacity fade exaggerates the negative effect of a slow charge. This indicates that, while capacity fade is necessary to retrieve the response to partial cycling seen in experiments, this particular degradation model is not sufficient. For a 3.4 Ah cell cycled at 0.3C/0.3C charge/discharge for 2600 s/3600 s from fully charged with a 2.21 V/2.38 V voltage cutoff: for case (i) without degradation, $k_s = 5 \times 10^{-5}$ s^{-1} a) voltage envelope from model without degradation; c) evolution of shuttling rate and of precipitated amount; and for case (ii) with degradation $k_s = 3 \times 10^{-5}$ s^{-1}, $f_s = 0.25$ b) voltage envelope from model with degradation; d) evolution of precipitated and lost sulfur.

Figure 9d, almost the entire precipitated amount is dissolved during a slow charge, while considerably increasing the amount of irreversibly lost material. The latter effect is strong enough to significantly shorten the duration of stage I of the cycling procedure with recovery.

Alternative mechanisms for capacity fade should be explored in the model, with a focus on retrieving the experimentally observed effect on cycling performance. For example, the irreversible oxidation of low order polysulfides to higher order species at the cathode side can also lead to reduced kinetics and capacity fade due to loss of active material.[30] As this occurs at low voltages, an irreversible precipitation-related loss could account for the three cycling stages seen in experiments without attributing a strong negative effect to a slow recovery charge. The effect of other precipitation-related irreversibility, such as caused by details of the crystallization/nucleation and growth of the precipitated material, or changes to microstructure could also be explored. It has been shown that polysulfides react with the electrolyte also in the absence of shuttle, leading to loss of active material, in a system with added shuttle suppressant $LiNO_3$ reached close to perfect Coulombic efficiency, but still suffered from capacity fade.[27]

Conclusions

Experimental data of LiS cells under capacity-limited partial cycling is used to develop an aging-aware model of a LiS cathode, and explore the mechanisms limiting the cell's cycle life. Cycling of LiS cells is shown experimentally to lead to voltage drift and apparent end of life, even when the Coulombic efficiency appears at its highest. Model predictions from a zero dimensional model confirm that this voltage drift is associated with a SoC drift, and emphasize the dangers of using coulomb counting or voltage reading for SoC estimation of LiS under cycling conditions. The model predicts the cell response is dominated by the interplay between charging inefficiencies due to shuttle and dissolution limitation during charging; the latter not only creates a bottleneck for the electrochemical reactions, but also leads to progressive accumulation of precipitation. While these conclusions are drawn from partial cycling data, they are also valid for complete cycles.

The model developed here is used to explain and verify the seemingly complex behavior under the capacity limited cycling, showing that many of the features observed are the result of the imposed constraints on operational parameters, such as the presence of the voltage cutoff. Some features can be retrieved only by a model with degradation, here implemented as loss of active material as a fraction of shuttled sulfur. The degradation-aware model indicates that

Reversible capacity loss occurs when, during charging, the precipitated amount does not fully re-dissolve; this is verified by the fact that applying a slow charge helps recover some of that capacity loss and

Irreversible capacity loss occurs when part of the active sulfur mass is lost, in this model due to shuttle; this can be verified by cycling the cell with a lower upper voltage cutoff, which shows improved cycle life, as shown in Supplementary material A.

These findings indicate that charging conditions are crucial to the true cell capacity and cycle life. Low rate charging leads to low charging efficiency and irreversible loss associated with shuttle. High rate charging leads to precipitate accumulation, and thus increased reversible capacity fade. The developed model can help distinguish between these two modes of capacity fade, and is thus an ideal platform for SoC estimation.

The degradation-aware model overestimates the negative effect of slow charging compared to the behavior seen in experiments. This indicates that a more complex description of degradation mechanisms is required. The model can become a quantitative tool to recommend operational parameters for improved cell longevity under various constraints, such as maximum energy or power per lifetime. The present work highlights the importance of studying the performance of LiS cells under realistic load cycles in accelerating their application-targeted improvement.

Acknowledgments

The authors thank the Engineering and Physical Sciences Research Council in the UK and Innovate UK for funding this work under the Revolutionary Electric Vehicle Battery (REVB) project 101573 and EP/L505298/1, and acknowledge useful discussions with Rajlakshmi Purkayastha from OXIS Energy.

ORCID

Monica Marinescu https://orcid.org/0000-0003-1641-3371
Teng Zhang https://orcid.org/0000-0002-3657-5151
Gregory J. Offer https://orcid.org/0000-0003-1324-8366

References

1. X. Ji and L. F. Nazar, *J. Mater. Chem.*, **20**, 9821 (2010).
2. L. F. Nazar, M. Cuisinier, and Q. Pang, *MRS Bull.*, **39**, 436 (2014).
3. I. A. Hunt, Y. Patel, M. Szczygielski, L. Kabacik, and G. J. Offer, *Journal of Energy Storage*, **2**, 25 (2015).
4. *European Consortium for Lithium-Sulfur Power for Space Environments*, http://cordis.europa.eu/project/rcn/199169_en.html, Accessed: 2017-04-03.
5. *Ultra Low Temperature Battery*, http://gtr.rcuk.ac.uk/projects?ref=132153, Accessed: 2017-04-03.
6. Y.-S. Su, Y. Fu, T. Cochell, and A. Manthiram, *Nat. Commun.*, **4**, 2985 (2013).
7. Y. Diao, K. Xie, S. Xiong, and X. Hong, *J. Power Sources*, **235**, 181 (2013).
8. M. R. Busche, P. Adelhelm, H. Sommer, H. Schneider, K. Leitner, and J. Janek, *J. Power Sources*, **259**, 289 (2014).
9. M. Marinescu, T. Zhang, and G. J. Offer, *Phys. Chem. Chem. Phys.*, **18**, 584 (2016).
10. J. Yan, X. Liu, and B. Li, *Adv. Sci.*, 1600101 (2016).
11. S. S. Zhang, *J. Electrochem. Soc.*, **159**, A920 (2012).
12. J. Zheng, D. Lv, M. Gu, C. Wang, J.-G. Zhang, J. Liu, and J. Xiao, *J. Electrochem. Soc.*, **160**, A2288 (2013).
13. J. Brückner, S. Thieme, H. T. Grossmann, S. Dörfler, H. Althues, and S. Kaskel, *J. Power Sources*, **268**, 82 (2014).
14. M. Hagen, D. Hanselmann, K. Ahlbrecht, R. Maça, D. Gerber, and J. Tübke, *Adv. Energy Mater.*, **5**, 1401986 (2015).
15. T. Poux, P. Novák, and S. Trabesinger, *J. Electrochem. Soc.*, **163**, A1139 (2016).
16. S. Risse, S. Angioletti-Uberti, J. Dzubiella, and M. Ballauff, *J. Power Sources*, **267**, 648 (2014).
17. A. F. Hofmann, D. N. Fronczek, and W. G. Bessler, *J. Power Sources*, **259**, 300 (2014).
18. T. Danner, G. Zhu, A. F. Hofmann, and A. Latz, *Electrochim. Acta*, **184**, 124 (2015).
19. K. Propp, D. J. Auger, A. Fotouhi, S. Longo, and V. Knap, *J. Power Sources*, **343**, 254 (2017).
20. H. Wang, N. Sa, M. He, X. Liang, L. F. Nazar, M. Balasubramanian, K. G. Gallagher, and B. Key, *J. Phys. Chem. C*, 6011 (2017).
21. M. S. Park, S. B. Ma, D. J. Lee, D. Im, S.-G. Doo, and O. Yamamoto, *Sci. Rep.*, **4**, 3815 (2014).
22. Y. V. Mikhaylik and J. R. Akridge, *J. Electrochem. Soc.*, **151**, A1969 (2004).
23. M. J. Lacey, A. Yalamanchili, J. Maibach, C. Tengstedt, K. Edström, and D. Brandell, *RSC Adv.*, **6**, 3632 (2016).
24. X.-B. Cheng, C. Yan, J.-Q. Huang, P. Li, L. Zhu, L. Zhao, Y. Zhang, W. Zhu, S.-T. Yang, and Q. Zhang, *Energy Storage Materials*, **6**, 18 (2017).
25. T. Zhang, M. Marinescu, L. O'Neill, M. Wild, and G. Offer, *Phys. Chem. Chem. Phys.*, **17**, 22581 (2015).
26. T. Zhang, M. Marinescu, S. Walus, and G. J. Offer, *Electrochim. Acta*, **219**, 502 (2016).
27. C. Barchasz, J.-C. Leprêtre, F. Alloin, and S. Patoux, *J. Power Sources*, **199**, 322 (2012).
28. T. Zhang, M. Marinescu, S. Walus, P. Kovacik, and G. J. Offer, *J. Electrochem. Soc.*, **165**, 6001 (2018).
29. K. Kumaresan, Y. Mikhaylik, and R. E. White, *J. Electrochem. Soc.*, **155**, A576 (2008).
30. Y. Diao, K. Xie, S. Xiong, and X. Hong, *J. Electrochem. Soc.*, **159**, A1816 (2012).